

# Homopolynuclear Tl<sup>I</sup> and Heteropolynuclear Au<sup>I</sup>–Tl<sup>I</sup> Complexes with Organodiselenone Ligands: Activation of Luminescence by Intermetallic Interactions

Massimiliano Arca,<sup>[a]</sup> Teresa Aroz,<sup>[b]</sup> M. Concepción Gimeno,<sup>[b]</sup> Monika Kulcsar,<sup>[b]</sup> Antonio Laguna,<sup>[b]</sup> Tania Lasanta,<sup>[c]</sup> Vito Lippolis,<sup>\*,[a]</sup> José M. López-de-Luzuriaga,<sup>\*,[c]</sup> Miguel Monge,<sup>[c]</sup> and M. Elena Olmos<sup>[c]</sup>

**Keywords:** Gold / Thallium / Selenium ligands / Luminescence / Density functional calculations

The organodiselenone ligands 1,1-bis(3-methyl-4-imidazolin-2-selone)methane (**L1**) and 1,2-bis(3-methyl-4-imidazolin-2-selone)ethane (**L2**) have been used for the synthesis of homopolynuclear Tl<sup>I</sup> [Tl(L)PF<sub>6</sub>]<sub>n</sub>·(mMeCN)<sub>n</sub> [L = **L1**, m = 1 (**1**); L = **L2**, m = 0 (**2**)] and discrete heteropolynuclear [Tl{Au(C<sub>6</sub>Cl<sub>5</sub>)<sub>2</sub>}(L)] [L = **L1** (**3**), **L2** (**4**)] complexes. The crystal structures of complexes **1** and **3** have been determined through X-ray diffraction studies. Complex **1** consists of alternating thallium(I) centres and bidentate Se-donor ligands that result in polymeric chains. The crystal structure of **3** is formed by [Tl(**L1**)]<sup>+</sup> cations and [Au(C<sub>6</sub>Cl<sub>5</sub>)<sub>2</sub>]<sup>−</sup> anions joined together by an unsupported Au...Tl interaction. Compounds **3** and **4** are

luminescent in the solid state at room temperature and at 77 K with lifetimes in the nanosecond range. DFT and time-dependent (TD)-DFT calculations have been carried out on different model systems including the free ligand **L1**, a representative model of complex **1** and a model system of complex **3**. The character of the frontier molecular orbitals and the TD-DFT prediction of the absorption spectra are used to explain the origin of the luminescence of complexes **3** and **4** as an admixture of metal–metal (Au–Tl)-to-ligand charge transfer (MMLCT) and intraligand (IL) transitions as observed experimentally.

## Introduction

As is well known, heavy atoms have a marked tendency to form polynuclear aggregates that feature metal...metal interactions with distances shorter than the sum of their van der Waals radii. This effect has been related, in the case of closed-shell metals, to correlation and relativistic effects, the latter being a minor component of interaction-energy stabilization. In the case of transition metals like Rh, Ir, Cr and so on, London dispersion forces have been invoked to explain such phenomena.<sup>[1]</sup> Particularly abundant is the case of gold(I)-containing multidimensional complexes, in which Au<sup>I</sup>...Au<sup>I</sup> (aurophilic) interactions are of a strength

comparable to that of hydrogen bonds.<sup>[2]</sup> Nevertheless, the availability and development of X-ray diffraction analyses has allowed us to show that gold(I) is not an exception in the periodic table and that other metal atoms with closed-shell configurations can display the same behaviour. Thus, examples of interactions between metal centres with d<sup>10</sup>–d<sup>10</sup>,<sup>[3–7]</sup> d<sup>8</sup>–d<sup>8</sup>,<sup>[8]</sup> and s<sup>2</sup>–s<sup>2</sup>,<sup>[9,10]</sup> configurations, or even between centres of different configurations such as s<sup>2</sup>–d<sup>8</sup>,<sup>[11–13]</sup> s<sup>2</sup>–d<sup>10</sup>,<sup>[14,15]</sup> and d<sup>8</sup>–d<sup>10</sup>,<sup>[16–19]</sup> have been reported and theoretical studies of selected examples have been carried out.<sup>[1,20]</sup> From these studies it has been concluded that Au<sup>I</sup> and Tl<sup>I</sup> represent the two extremes of metallophilicity and, thus, whereas aurophilic attractions can be considered the upper extreme of the metallophilic attractions with values up to 46 kJ mol<sup>−1</sup>, interactions that involve Tl<sup>I</sup> centres appear to be the weakest ones, even below 20 kJ mol<sup>−1</sup>.<sup>[21]</sup> The theoretical explanation of these values is that whereas aurophilic Au<sup>I</sup>...Au<sup>I</sup> attractions are enhanced by relativistic effects, these effects weaken the van der Waals attractions between the s<sup>2</sup> metal atoms.<sup>[22]</sup> Nevertheless, we have reported some products that contain both Au<sup>I</sup> and Tl<sup>I</sup> metal centres at distances shorter than the sum of their van der Waals radii (3.62 Å)<sup>[23]</sup> that are surprisingly stable. For instance, we have described metallophilicity between gold(I) and thallium(I) centres that make use of an acid–base synthetic strategy that involves bis(perhalophenyl)aurate(I) precur-

[a] Dipartimento di Chimica Inorganica ed Analitica, Università degli Studi di Cagliari, S.S. 554 Bivio per Sestu, 09042 Monserrato (CA), Italy Fax: +39-070-6754456 E-mail: lippolis@unica.it

[b] Departamento de Química Inorgánica, Instituto de Ciencia de Materiales de Aragón, Universidad de Zaragoza – CSIC, 50009 Zaragoza, Spain

[c] Departamento de Química, Universidad de La Rioja, Grupo de Síntesis Química de La Rioja, UA-CSIC, Complejo Científico-Tecnológico, 26004 Logroño, Spain Fax: +34-941-299-621 E-mail: josemaria.lopez@unirioja.es

Supporting information for this article is available on the WWW under <http://dx.doi.org/10.1002/ejic.201100004>.

sors and acid Tl<sup>I</sup> salts, thereby finding interaction energies as high as 276 kJ mol<sup>-1</sup>, of which 80% is determined by an ionic interaction.<sup>[24]</sup>

In addition to the intriguing nature of this interaction from a theoretical viewpoint, it can be considered to be responsible for very important physical properties of the materials that contain it, for example, luminescence.<sup>[25]</sup> In those systems, this property is strongly dependent on the environment around the metal centres, the metal–metal distances and the nature of ligands bonded to them. In this regard, thallium(I) displays an astonishing complexity in coordination numbers and geometries,<sup>[26]</sup> which may also imply that different vacant coordination sites are available for interaction with a wide variety of substrates. In this way, we have prepared heteronuclear gold–thallium systems with different dimensionality (from single molecules to 1D, 2D and 3D polymers), and donor ligands bonded to thallium, for instance, O-donor (OPPh<sub>3</sub>, ketones, DMSO, DMF, THF, β-diketonates), N-donor (aliphatic and aromatic amines) or C-donor (toluene).<sup>[27]</sup> From all these examples it can be deduced that thallium(I) shows a preference for ligands that bear hard donor atoms, but reactivity with ligands with donor centres of lower periods is an unexplored area. Therefore, continuing with these studies we wondered whether this metal atom is suitable for coordination to other ligands with softer donor characteristics—for instance, selenium-donor ligands—to increase knowledge about the influence of the ligands on the structure and the luminescence of systems that feature Au<sup>I</sup>⋯Tl<sup>I</sup> metallophilic interactions.

In this paper we describe the synthesis, characterization and study of the photophysical properties of thallium(I) and heteronuclear gold(I)–thallium(I) complexes with the bidentate selenium ligands 1,1-bis(3-methyl-4-imidazolin-

2-selone)methane (**L1**) and 1,2-bis(3-methyl-4-imidazolin-2-selone)ethane (**L2**). It is also important to add that very few metal complexes of these types of Se-donor ligands are reported in the literature.<sup>[28]</sup>

## Results and Discussion

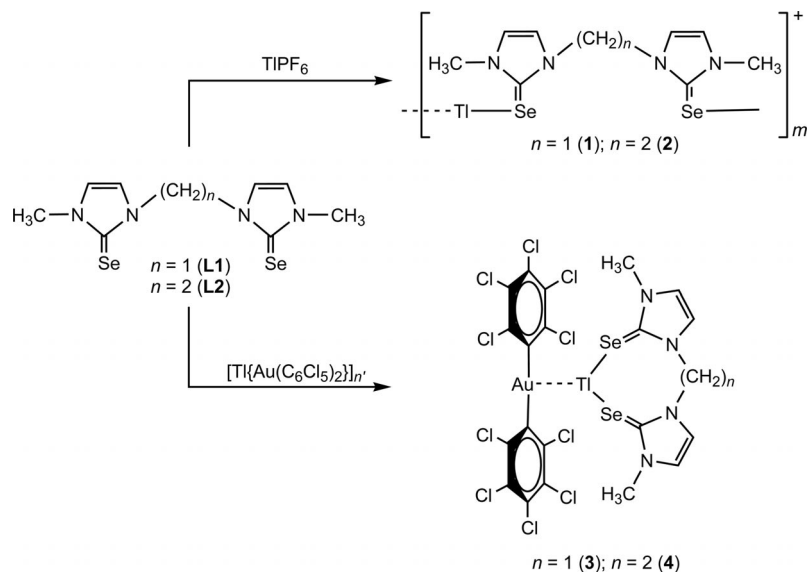
### Synthesis and Characterization

Compounds [Tl(L)PF<sub>6</sub>]<sub>*n*</sub>(*m*MeCN)<sub>*n*</sub> [**L** = **L1**, *m* = 1 (**1**), **L** = **L2**, *m* = 0 (**2**)] and [Tl{Au(C<sub>6</sub>Cl<sub>5</sub>)<sub>2</sub>}(L)] [**L** = **L1** (**3**), **L2** (**4**)] were obtained by reaction of TlPF<sub>6</sub> or [Tl{Au(C<sub>6</sub>Cl<sub>5</sub>)<sub>2</sub>}]<sub>*n*</sub> and equimolecular amounts of the organodiselenone ligands by using MeCN or tetrahydrofuran as solvent (see Scheme 1).

Complexes **1** and **2** were obtained as white crystalline solids by evaporation of acetonitrile and further washing with diethyl ether. Complexes **3** and **4** were isolated as orange solids and were insoluble in solvents with low coordinating ability, such as dichloromethane, toluene, acetonitrile or diethyl ether, and soluble in tetrahydrofuran or acetone. All complexes were stable to air and moisture for long periods of time. Analytical and spectroscopic data of all complexes agree with the proposed stoichiometries (see the Exp. Section).

The <sup>1</sup>H NMR spectra of complexes **1** and **2** in [D<sub>6</sub>]-DMSO and **3** and **4** in [D<sub>6</sub>]acetone display the corresponding ligand signals (see the Experimental Section).

Mass spectra show signals that correspond to [Au(C<sub>6</sub>Cl<sub>5</sub>)<sub>2</sub>]<sup>-</sup> at *m/z* = 695 (MALDI<sup>-</sup>) and [Tl(L)]<sup>+</sup> at *m/z* = 534 (**L** = **L1**) and *m/z* = 553 (**L** = **L2**) (MALDI<sup>+</sup>) with the expected isotopic distributions, but other peaks of higher nuclearity were not detected.



Scheme 1. Synthesis of complexes **1–4**.

## X-ray Structural Determination of Derivatives 1 and 3

Single crystals of complex **1** suitable for X-ray diffraction studies were obtained by slow diffusion of hexane into a solution of the complex in acetonitrile. It crystallizes in the space group *Pbca* of the orthorhombic system with one molecule of acetonitrile per thallium atom. Its crystal structure is formed by alternating thallium(I) centres and bidentate Se-donor ligands that result in polymeric chains that run parallel to the crystallographic *y* axis, which are further connected by weaker Tl–Se bonds, thereby resulting in the formation of sheets perpendicular to the *z* axis (Figure 1). The Tl–Se bond lengths (Table 1) within the one-dimensional polymers [3.0929(6) and 3.2127(6) Å] are similar to those previously reported for complexes  $[(C_4H_9)_4N]_2[Tl_2\{Se_2C=C(CN)_2\}_2] \cdot 2(CH_3)_2CO$  (3.132–3.207 Å)<sup>[29]</sup> and  $[AsPh_4]_2[Tl_2\{Se_2C=C(CN)_2\}_2]$  (3.108–3.162 Å),<sup>[30]</sup> which are shorter than those found between thallium and selenium atoms of adjacent chains in **1** [3.335(1) and 3.404(1) Å] [ $\Sigma_{vdw}(Tl-Se) = 3.86$  Å].<sup>[23]</sup> The Tl–Tl distance of 5.504(1) Å is much longer than those observed in the crystal structures that feature the anionic species  $[Tl_2\{Se_2C=C(CN)_2\}_2]^{2-}$  [3.570(1)<sup>[29]</sup> and 3.547 Å<sup>[30]</sup>] and also longer than the double of the van der Waals radius of thallium (3.92 Å),<sup>[23]</sup> which indicates the absence of any type of interaction between the metal atoms in **1**.

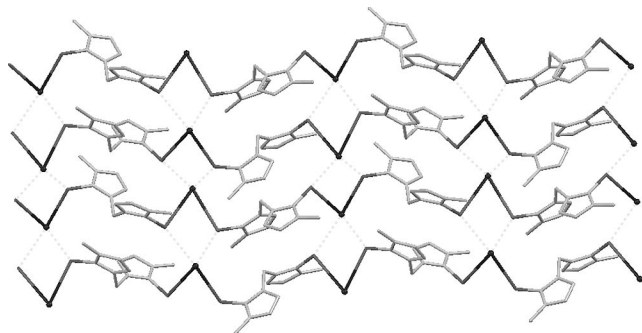


Figure 1. View of the two-dimensional structure of complex **1**. Hydrogen atoms, counteranions and co-crystallized MeCN molecules have been omitted for clarity.

Table 1. Selected bond lengths [Å] and angles [°] for the complex cation  $[Tl(L1)]^+$  in the crystal structure of complex **1**.<sup>[a]</sup>

Tl(1)–Se(1)	3.2127(6)	Tl(1)–Se(2)#1	3.335(1)
Tl(1)–Se(2)	3.0929(6)	Se(1)–C(1)	1.854(4)
Tl(1)–Se(1)#1	3.404(1)	Se(2)–C(5)	1.861(4)
Se1–Tl1–Se2	60.13(1)	Tl1–Se1–Tl1#2	112.54(1)
Se1–Tl1–Se2#1	64.724(17)	Tl1–Se2–Tl1#2	117.75(1)
Se1–Tl1–Se1#1	81.02(1)	C1–Se1–Tl1	108.51(13)
Se2–Tl1–Se2#1	89.20(1)	C5–Se2–Tl1	102.69(14)

[a] Symmetry transformations used to generate equivalent atoms: #1:  $x + \frac{1}{2}, y, -z + \frac{1}{2}$ ; #2:  $x - \frac{1}{2}, y, -z + \frac{1}{2}$ .

The additional presence of secondary interactions of different nature between these cationic sheets,  $PF_6^-$  anions and solvent MeCN molecules gives rise to a 3D arrangement, as shown in Figure 2. In particular, each thallium maintains

two Tl $\cdots$ F contacts of 3.336 and 2.897 Å with fluorine atoms of the same  $PF_6^-$  anion [ $\Sigma_{vdw}(Tl-F) = 3.43$  Å]<sup>[23]</sup> and one Tl $\cdots$ N contact of 3.154 Å with the nitrogen centre of an acetonitrile molecule [ $\Sigma_{vdw}(Tl-N) = 3.51$  Å],<sup>[23]</sup> as shown in Figure 3. Additionally, C–H $\cdots$ F hydrogen bonds between the solvent or the Se-donor ligand and  $PF_6^-$  anions, which are the responsible for the further dimensionality of the network, are observed (Figure 2).

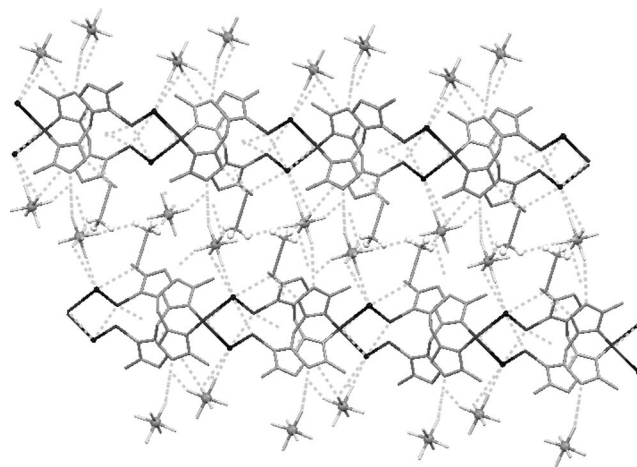


Figure 2. 3D network in the crystal structure of complex **1** built through Tl $\cdots$ F, Tl $\cdots$ N and C–H $\cdots$ F contacts.

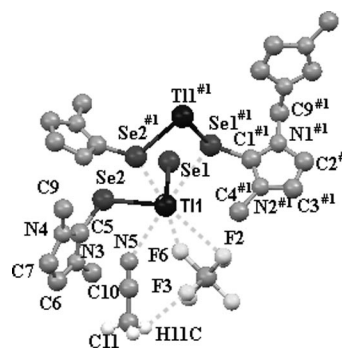


Figure 3. Environment of the thallium(I) atom in the crystal structure of complex **1** with the labelling scheme for the atom positions.

The crystal structure of complex **3** was determined from single crystals obtained by slow diffusion of hexane into a solution of the complex in tetrahydrofuran. The most interesting feature in this structure is the modification of the coordination mode of the bidentate Se-donor ligand, which now acts as chelating instead of bridging ligand, as in **1**, presumably as a consequence of the incorporation of the gold(I) atom of the bis(aryl)aurate(I) anion into the coordination sphere of thallium. Thus, the crystal structure of **3** is formed by  $[Tl(L1)]^+$  cations and  $[Au(C_6Cl_5)_2]^-$  anions joined together by an unsupported Au $\cdots$ Tl interaction, as shown in Figure 4. The Au–Tl distance of 2.9619(8) Å compares well with the shortest one found in  $[Tl\{Au(C_6Cl_5)_2\}(tmda)]_n$  (*tmda* = tetramethylenediamine) [2.9782(4) Å]<sup>[31]</sup> and lies within the range of Au–Tl distances observed in other re-

lated polynuclear Au/Tl systems with unsupported metal-metal interactions [2.9078(3)–3.3205(3) Å].<sup>[24,25a,25b,32–39]</sup> The Tl⋯Se bond lengths (Table 2) have values of 3.0471(16) and 3.1936(17) Å. The former is shorter than those found in **1** [3.0929(6) and 3.2127(6) Å] or in the related compounds [(C<sub>4</sub>H<sub>9</sub>)<sub>4</sub>N]<sub>2</sub>[Tl<sub>2</sub>{Se<sub>2</sub>C=C(CN)<sub>2</sub>}<sub>2</sub>]·2(CH<sub>3</sub>)<sub>2</sub>CO (3.132–3.207 Å)<sup>[29]</sup> and [AsPh<sub>4</sub>]<sub>2</sub>[Tl<sub>2</sub>{Se<sub>2</sub>C=C(CN)<sub>2</sub>}<sub>2</sub>] (3.108–3.162 Å),<sup>[30]</sup> whereas the second one compares well with most of the Tl–Se bond lengths noted. The environment at thallium is trigonal pyramidal with two positions occupied by the selenium donors from the ligand **L1**, and the third coordination site occupied by the anion [Au(C<sub>6</sub>Cl<sub>5</sub>)<sub>2</sub>]<sup>–</sup> in which the gold centre shows its characteristic linear environment by the coordination of the pentachlorophenyl groups with typical Au–C distances of 2.051(15) and 2.062(16) Å.

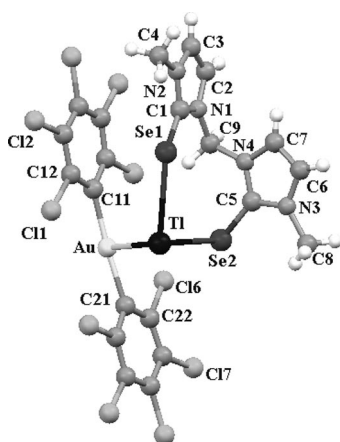


Figure 4. Asymmetric unit of the crystal structure of complex **3** with the labelling scheme for the atom positions.

These heterodinuclear Au<sup>I</sup>/Tl<sup>I</sup> complexes are further connected into pairs thanks to the presence of two Tl⋯Se interactions of 3.433(2) Å, and one Se⋯Se contact of 3.674(3) Å. Additionally, each selenium atom acts as acceptor of a highly directional C–H⋯Se hydrogen bond [C9⋯Se 3.83(2), H⋯Se 2.86(1) Å, C9–H⋯Se 171.3(9)°], which is the responsible for the expansion of the structure into a polymeric

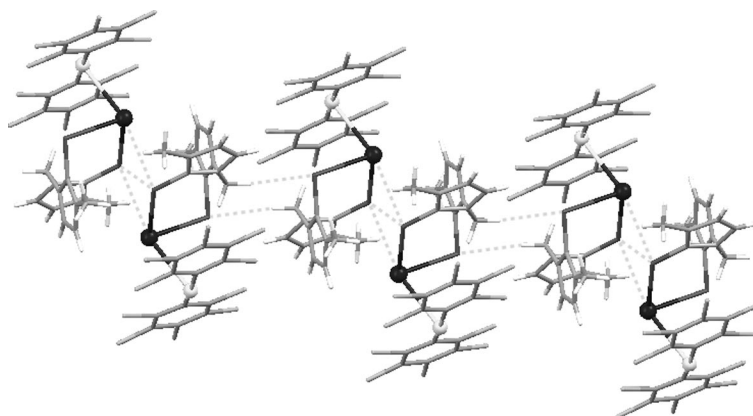


Figure 5. View of the polymeric chain structure of complex **3** built through C–H⋯Se hydrogen bonds.

Table 2. Selected bond lengths [Å] and angles [°] for complex **3**.

Au–C11	2.051(15)	Tl–Se1	3.1936(17)
Au–C21	2.062(16)	Se1–C1	1.811(16)
Au–Tl	2.9619(8)	Se2–C5	1.845(15)
Tl–Se2	3.0471(16)		
C11–Au–C21	175.9(6)	Au–Tl–Se1	107.90(4)
C11–Au–Tl	88.2(4)	Se2–Tl–Se1	97.12(4)
C21–Au–Tl	88.5(4)	C1–Se1–Tl	128.2(5)
Au–Tl–Se2	79.05(4)	C5–Se2–Tl	94.9(4)

chain, as is shown in Figure 5 (the structural features of the C–H⋯Se hydrogen bond in **3** fall in the range found for similar contacts that involve aliphatic methylene hydrogen atoms and selenium atoms<sup>[40]</sup>). The free coordination hemisphere around the Tl<sup>I</sup> centre might be indicative of the presence of a stereochemically active 6s<sup>2</sup> lone pair.

### Photophysical Studies and DFT and Time-Dependent (TD)-DFT Calculations

The absorption spectra of the organodiselenone ligands **L1** and **L2**, at  $2 \times 10^{-5}$  M concentration in chloroform, show an intense featureless band at 287 nm ( $\epsilon = 23670 \text{ M}^{-1} \text{ cm}^{-1}$ ) and 281 nm ( $\epsilon = 27260 \text{ M}^{-1} \text{ cm}^{-1}$ ), respectively (Figure 6). Complexes **1** and **2** show an absorption band in acetone at  $2 \times 10^{-5}$  M concentration at 209 and 214 nm ( $\epsilon = 60000 \text{ M}^{-1} \text{ cm}^{-1}$ ), respectively. These energies are similar to those of the ligands **L1** and **L2**, thus suggesting a similar origin. In contrast, the heteropolynuclear complexes **3** and **4**, which are insoluble in chloroform, display an intense absorption band in  $1 \times 10^{-3}$  M acetone solution at 330 nm ( $\epsilon = 1594 \text{ M}^{-1} \text{ cm}^{-1}$ ) (**3**) and 330 nm ( $\epsilon = 1543 \text{ M}^{-1} \text{ cm}^{-1}$ ) (**4**), and an additional shoulder (Figure 6) at around 430 nm ( $\epsilon = 200 \text{ M}^{-1} \text{ cm}^{-1}$ ) for both complexes. The similarity between the high-energy bands of these complexes with the absorption band of the free ligands suggests a similar origin.

From all the noted compounds and ligands, the only ones that show an emissive behaviour are the heteronuclear gold(I)–thallium(I) complexes **3** and **4**. Thus, complexes **3** and **4** emit at 603 nm (exc. 488 nm) (**3**) and at 660 nm (exc. 556 nm) (**4**) in the solid state at room temperature and at

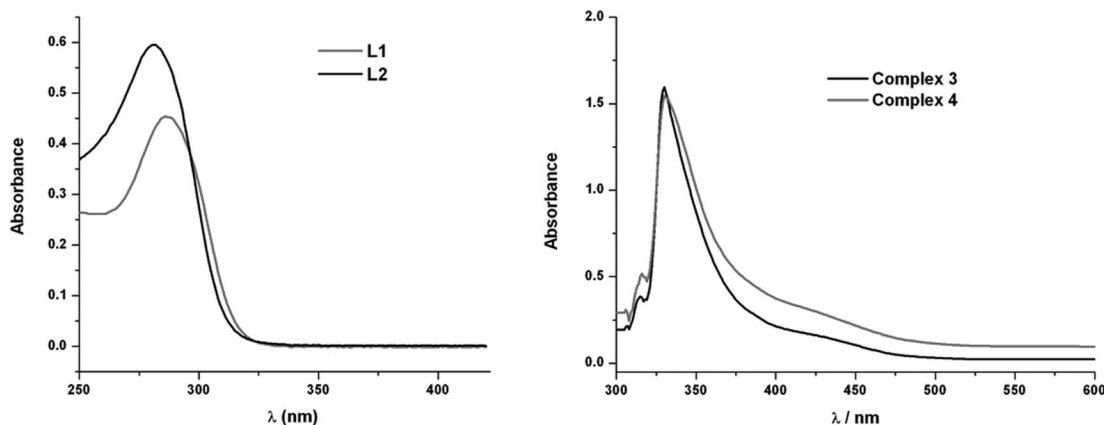


Figure 6. UV/Vis absorption spectra for solutions of **L1** and **L2** in  $2 \times 10^{-5}$  M  $\text{CHCl}_3$  and for solutions of complexes **3** and **4** in  $1 \times 10^{-3}$  M acetone.

617 nm (exc. 456 nm) (**3**) and at 667 nm (exc. 487 nm) (**4**) in the solid state at 77 K (Figure 7). The lifetime of the emission in the solid state at room temperature displays two components within the nanosecond timescale for both complexes:  $\tau_1 = 119$  ns,  $\tau_2 = 514$  ns (**3**) and  $\tau_1 = 50$  ns,  $\tau_2 = 435$  ns (**4**), thereby indicating that the emissions probably originate from excited states of singlet parentage and consequently are both tentatively assigned as fluorescence. The behaviour of these complexes in solution is different and does not show luminescence; it is recovered when the solvent is evaporated without apparent degradation of the sample. This fact suggests that the gold(I)–thallium(I) interaction influences the optical properties of this material and probably the rupture of the interaction by the solvent quenches the emission. In this regard, related complexes that show gold–thallium interactions usually show luminescence assigned to transitions that originate in these interactions, the rupture of which provokes its quenching.<sup>[27]</sup> Moreover, it is worth mentioning that upon increasing the concentration in solution, both complexes **3** and **4** display emissions that can be assigned to the formation of metallophilic interactions in solution. Despite the fact we have detected luminescence in polymeric complexes that bear only thallium (I) centres such as  $[\text{Tl}(\text{acac})]$  (acac = acetyl-

acetate),<sup>[32]</sup> in the case of complexes **1** and **2** we do not observe emissive properties under the same conditions. This fact would be related to the absence of  $\text{Tl}^{\text{I}}\text{–Tl}^{\text{I}}$  interactions in the latter complexes, which were assigned as the origin of the luminescence in the former or even in heteronuclear gold(I)–thallium(I) compounds that show both types of interactions ( $\text{Au}^{\text{I}}\text{–Tl}^{\text{I}}$  and  $\text{Tl}^{\text{I}}\text{–Tl}^{\text{I}}$ ).<sup>[41]</sup>

DFT and TD-DFT calculations on model systems of the previously noted compounds have been carried out. We first studied the electronic structure of models **L1a**, **1a** and **3a** obtained through DFT optimization in the case of **L1a** and single-point DFT calculations in the case of models **1a** and **3a**. These three models represent the experimental structures of the free ligands **L1** and **L2**, the polymeric thallium complexes **1** and **2** and the heteropolynuclear  $\text{Au}^{\text{I}}\text{–Tl}^{\text{I}}$  compounds **3** and **4**, respectively. With these results, we could check the shape of the frontier molecular orbitals and hence the contribution of each part of the molecules to these molecular orbitals (Figure 8). These calculations were carried out using both the B3-LYP and BH-LYP functionals.

The analysis of the frontier orbitals of model system **L1a** shows that the highest occupied molecular orbitals are mostly located at the selenium atoms with some contribution in HOMO and HOMO–1 from the imidazoline

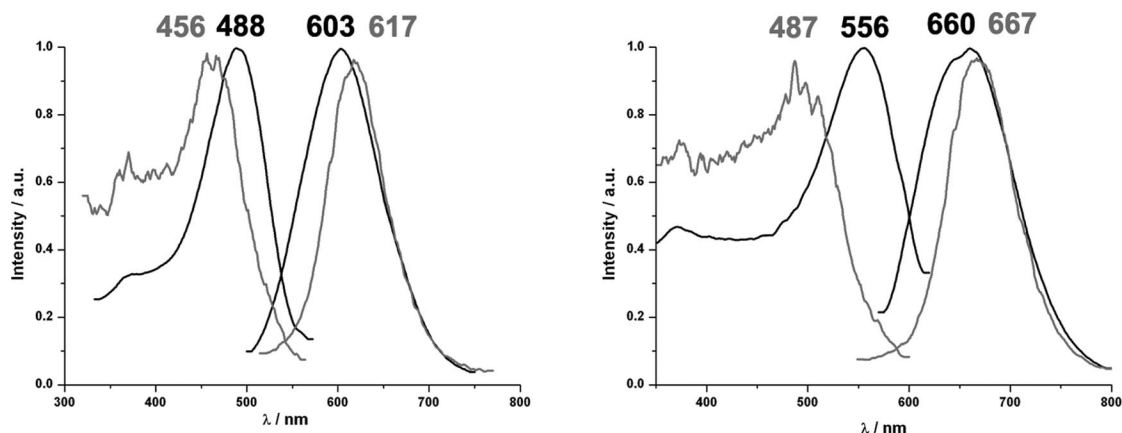


Figure 7. Excitation and emission spectra for complexes **3** (left) and **4** (right) in the solid state at room temp. (black) and at 77 K (grey).

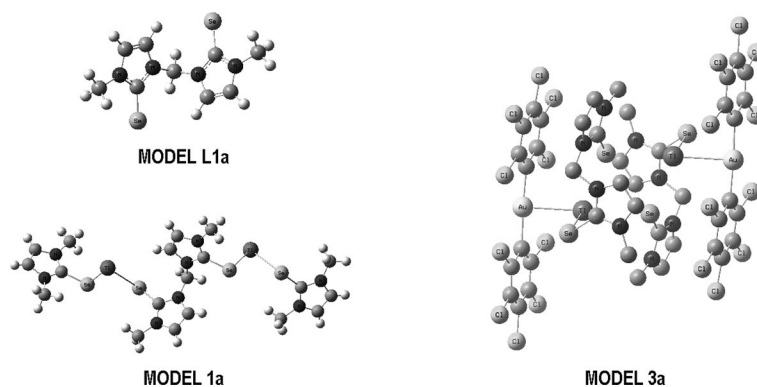


Figure 8. Theoretical model systems.

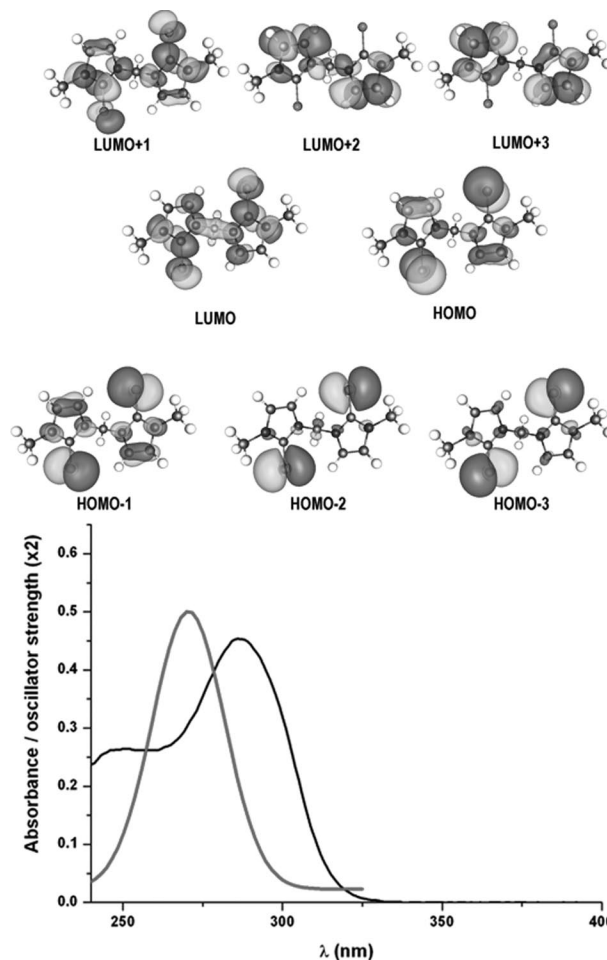
rings. On the other hand, the lowest unoccupied molecular orbitals are mostly placed at the imidazoline rings with some contribution in LUMO and LUMO+1 of the selenium atoms. The TD-DFT (B3-LYP) calculations of the first twenty singlet transitions show a very good agreement between the theoretical excitations and the experimental ones. The theoretical excitations (Table 3) display the contribution of the frontier orbitals to each excitation and the corresponding intensity (oscillator strength) (Figure 9), which shows that mainly  $n(\text{Se}) \rightarrow \pi^*(\text{ring})$  transitions are responsible for the absorption observed experimentally.

Table 3. TD-DFT singlet excitation calculations for model system **L1a**.

Excitation	$\lambda_{\text{calcd.}}$ [nm]	Osc. str. <sup>[a]</sup>	Contributions <sup>[b]</sup>
A	289.1	0.0743	HOMO $\rightarrow$ LUMO (84.8)
B	273.5	0.0111	HOMO $\rightarrow$ LUMO+1 (45.2) HOMO-2 $\rightarrow$ LUMO+1 (23.7)
C	268.3	0.0433	HOMO-3 $\rightarrow$ LUMO+1 (44.3) HOMO-2 $\rightarrow$ LUMO (28.9)
D	261.5	0.1822	HOMO-1 $\rightarrow$ LUMO+1 (54.3) HOMO-3 $\rightarrow$ LUMO+1 (25.3)
E	258.4	0.0125	HOMO $\rightarrow$ LUMO+2 (78.4)
F	251.8	0.0942	HOMO $\rightarrow$ LUMO+3 (68.1) HOMO-1 $\rightarrow$ LUMO+2 (22.2)
G	247.1	0.0115	HOMO-2 $\rightarrow$ LUMO+3 (88.4)

[a] The oscillator strength shows the mixed representation of both velocity and length representations. [b] The value is  $|\text{coeff.}|^2 \times 100$ .

The DFT and TD-DFT analyses of a model system (**1a**) (Figure 10), which represents the polymeric arrangement found for complexes **1** and **2** in the solid state, show different features. In this case, the shape of the highest-occupied molecular orbitals is similar to that of the free ligand, and therefore they are mostly located at the selenium atoms with some contribution of the ligand rings. However, the analysis of the lowest unoccupied molecular orbitals displays a main contribution of the thallium atoms, which would suggest a ligand-to-metal charge-transfer transition for the absorption of these complexes. Nevertheless, the similarity of the absorption spectra of the complexes **1** and **2** and those of the free ligands would suggest a breaking of the thallium–ligand bonds in acetone, thus leading to the above-mentioned intraligand transitions. The TD-DFT analysis of model system **1a** shows low-intensity theoretical

Figure 9. Frontier molecular orbitals for the free ligand model system **L1a** and experimental (black) versus theoretical absorption spectra (grey).

excitations (see the Supporting Information), which are likely to preclude an emissive behaviour of this complex in the solid state as it is observed experimentally (see above). In any case, the difference between the theoretical model system and the 3D experimental structure does not allow us to reproduce all the interactions experimentally found in the theoretical analysis. Therefore the discrepancy between

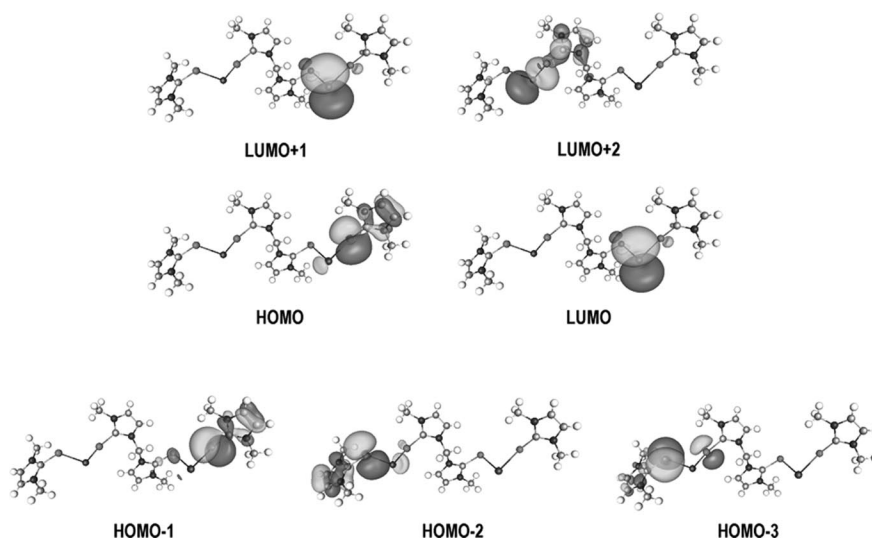


Figure 10. Frontier molecular orbitals for model system **1a**.

theoretical and experimental values could be due to this fact.

By contrast, the DFT electronic structure of the frontier orbitals for the model system **3a** displays interesting differences. Thus, the highest occupied molecular orbital HOMO and HOMO–1 are both located at the interacting gold–thallium atoms and at the ligands, thus showing the importance of the gold–thallium interaction in the photophysics of these systems. The population analysis of these highest occupied molecular orbitals shows that the Au–Tl interacting metals contribute to the molecular orbitals in a 36% in the case of HOMO and 29% in the case of HOMO–1, which is a contribution larger than that of lower energy occupied orbitals. With regards to the empty orbitals LUMO to LUMO+3, we observe a main contribution of the selenium-donor ligands (LUMO) with some contribution from the thallium centres and the C<sub>6</sub>Cl<sub>5</sub> rings (LUMO+1 to LUMO+3). The TD-DFT calculations of the first ten singlet excitations show interesting trends (see Table 4). The energy and intensity of these theoretical transitions resemble the low-energy shoulder observed experimentally in the absorption spectrum (Figure 11). Moreover, the excitation-energy profile for this complex matches the low-energy part of the absorption spectrum. Therefore, we could tentatively assign these theoretical transitions to the origin of the emission in this complex. A deeper investigation of the theoretical transitions shows the orbital contribution to the theoretical excitations. The most intense theoretical excitations (A to E) arise from HOMO and HOMO–1 orbitals to LUMO to LUMO+3.

In view of these results, an admixture of metal–metal (Au–Tl)-to-ligand charge transfer (MMLCT) and intraligand (IL) transitions would be the origin of the luminescent behaviour of complexes **3** and **4**.

To test the validity of our results, we repeated the TD-DFT calculations using a different functional as BH-LYP. We found in all cases quite similar excitation profiles for the model systems **L1a** and **3a** but blueshifted in energy (see

Table 4. TD-DFT singlet excitation calculations for model system **3a**.

Excitation	$\lambda_{\text{calcd.}}$ [nm]	Osc. strength <sup>[a]</sup>	Contributions <sup>[b]</sup>
A	428	0.0063	HOMO→LUMO+1 (48.3) HOMO→LUMO (32.1)
B	424.7	0.022	HOMO→LUMO (31.0) HOMO–1→LUMO+1 (25.2) HOMO–1→LUMO+2 (15.0)
C	420.7	0.016	HOMO–1→LUMO+2 (33.5) HOMO–1→LUMO+3 (21.3) HOMO→LUMO+2 (21.3)
D	414.8	0.027	HOMO→LUMO+2 (55.3) HOMO–1→LUMO+2 (26.9)
E	412.8	0.029	HOMO–1→LUMO+3 (63.8) HOMO→LUMO+3 (18.3)
F	398	0.0028	HOMO–2→LUMO (93.2)

[a] The oscillator strength shows the mixed representation of both velocity and length representations. [b] The value is  $|\text{coeff.}|^2 \times 100$ .

the Supporting Information). For thallium complex **1**, we observed a clear difference in the shape and energy of the theoretical absorption spectra, the one obtained through the BH-LYP functional being closer to the experimental values (see the Supporting Information).

## Conclusion

The use of organodiselenone ligands **L1** and **L2** has permitted the synthesis of homopolynuclear polymeric Tl<sup>I</sup> complexes and heterodinuclear Au<sup>I</sup>–Tl<sup>I</sup> compounds. In the latter, the solid-state structure consists of discrete [Tl{Au(C<sub>6</sub>Cl<sub>5</sub>)<sub>2</sub>}(L)] (L = **L1** or **L2**) molecules. Only in the case of the gold–thallium complexes is the luminescence activated, thereby displaying an admixture of metal–metal (Au–Tl)-to-ligand charge transfer (MMLCT) and intraligand (IL) transitions. Therefore, it could be said that the presence of gold(I) in these complexes switches on the “emissive properties” of the Tl<sup>I</sup> complexes of the organodiselenone ligands.

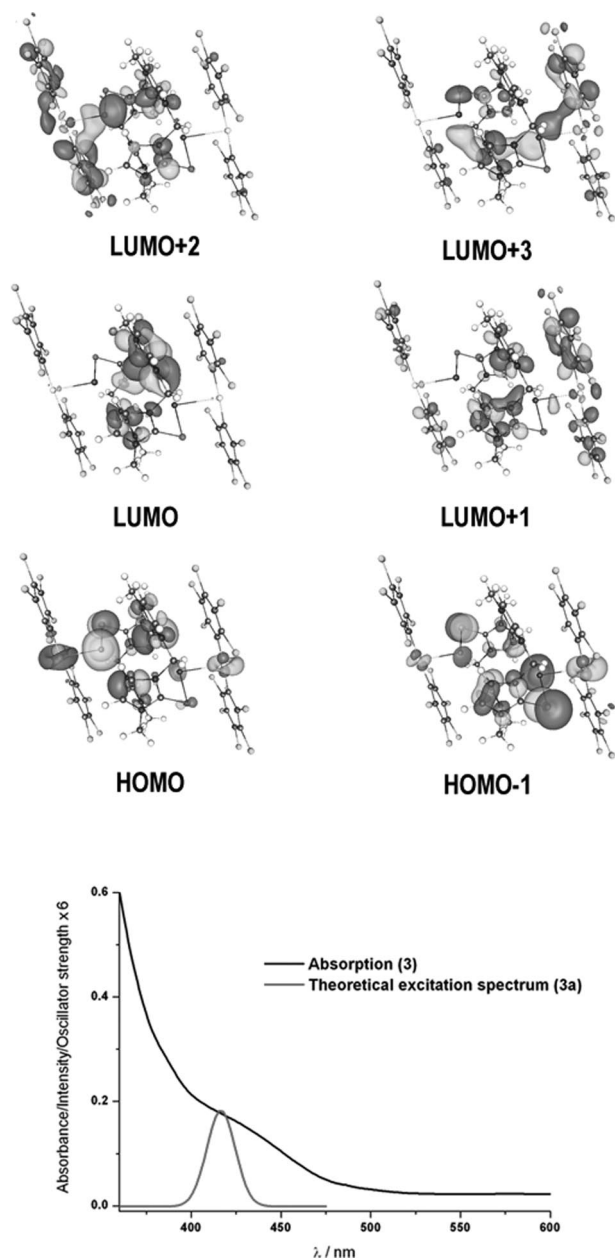


Figure 11. Frontier molecular orbitals for model system **3a** and experimental versus theoretical excitation spectra in the low-energy region.

## Experimental Section

**General:** Solvents were freshly distilled under argon prior to use and all the reactions were carried out under argon. Organic reagents and metal salts were purchased from Sigma Aldrich and used as received.  $[\text{Tl}\{\text{Au}(\text{C}_6\text{Cl}_5)_2\}]_n$  was prepared according to the literature.<sup>[25a]</sup>

**Instrumentation:** C and H analyses were carried out with a Perkin-Elmer 240C microanalyzer. Mass spectra were recorded with a Bruker Microflex MALDI-TOF using dithranol (DIT) or 1,1-dicyano-4-*tert*-butylphenyl-3-methylbutadiene (DCTB) as matrix. <sup>1</sup>H NMR spectra were recorded with a Bruker Avance 400 or a Bruker ARX 300 in  $[\text{D}_6]\text{DMSO}$  or  $[\text{D}_6]\text{acetone}$  solutions. Chemical shifts are quoted relative to  $\text{SiMe}_4$  (<sup>1</sup>H, external),  $\text{CFCl}_3$  (<sup>19</sup>F, external)

and  $\text{H}_3\text{PO}_4$  (85%) (<sup>31</sup>P, external). Excitation and emission spectra in the solid state were recorded with a Jobin-Yvon Horiba Fluorolog 3-22 Tau-3 spectrofluorimeter. Lifetime measurements were recorded with a DataStation HUB-B with a nanoLED controller and DAS6 software. The nanoLEDs employed for lifetime measurements were 370 nm with pulse lengths of 0.8–1.4 ns. The lifetime data were fitted with the Jobin-Yvon software package. Measurements at 77 K were done with an Oxford Cryostat Optistat DN with an accessory for solid samples.

**L1 and L2:** The synthesis of the organodiselenone ligands, 1,1-bis(3-methyl-4-imidazol-2-selone)methane (**L1**) and 1,2-bis(3-methyl-4-imidazol-2-selone)ethane (**L2**) were performed according to the literature.<sup>[42a]</sup> The process consists of two steps: synthesis of the appropriate 3-methylimidazolium bis-cation salt, and its reaction with elemental selenium in methanol in the presence of slight excess amount of  $\text{K}_2\text{CO}_3$ . We have improved the overall yield of this synthetic procedure by preparing quantitatively the required 3-methylimidazolium bis-cation salts from the reaction of 1-methylimidazole and an excess amount of the appropriate terminal dihalide under solvent-free and refluxing conditions.<sup>[42b]</sup> The use of solvent (AcOEt, THF) and of stoichiometric quantities of the reactants in this step generally causes a significant lowering of the yield in the 3-methylimidazolium bis-cation salt intermediate.

$\{[\text{Tl}(\text{L1})\text{PF}_6]_n \cdot \text{MeCN}\}_n$  (**1**) and  $\{[\text{Tl}(\text{L2})\text{PF}_6]_n$  (**2**):  $\text{TlPF}_6$  (0.042 g, 0.12 mmol) was added to a solution of **L1** (0.04 g, 0.12 mmol) or **L2** (0.04 g, 0.12 mmol) in MeCN (20 mL) and the reaction mixture was stirred for 24 h at room temperature. The solvent was removed under vacuum and the remaining white solid was washed with  $\text{Et}_2\text{O}$  and filtered off. Product **1** was recrystallized from  $\text{CH}_3\text{CN}/n$ -hexane (1:5 v/v). Compound **2** was obtained using the same workup.

**Compound 1:** Yield 0.069 g (85%).  $\text{C}_9\text{H}_{12}\text{TlF}_6\text{N}_4\text{PSe}_2 \cdot (\text{MeCN})$ ; calcd. C 18.23, H 2.09, N 9.67; found C 18.29, H 1.81, N 9.75. <sup>1</sup>H NMR (DMSO, 400 MHz):  $\delta$  = 3.56 (s, 6 H,  $-\text{CH}_3$ ), 6.33 (s, 2 H,  $-\text{CH}_2-$ ), 7.34 (d, 2 H,  $-\text{CH}=\text{CH}-$ , <sup>3</sup>*J*(H,H) = 2.3 Hz), 7.76 (d, 2 H,  $-\text{CH}=\text{CH}-$ , <sup>3</sup>*J*(H,H) = 2.3 Hz) ppm. <sup>31</sup>P{<sup>1</sup>H} NMR (DMSO, 161.9 MHz):  $\delta$  = -144.1 (q, 1 P) ppm. <sup>19</sup>F NMR (DMSO, 376.48 MHz):  $\delta$  = -70.1 (d, 6 F, <sup>1</sup>*J*(P,F) = 711.3 Hz) ppm.

**Compound 2:** Yield 0.062 g (78%).  $\text{C}_{10}\text{H}_{14}\text{F}_6\text{N}_4\text{PSe}_2\text{Tl}$  (697.50); calcd. C 17.22, H 2.02, N 8.03; found C 17.22, H 1.86, N 8.59. <sup>1</sup>H NMR (DMSO, 400 MHz):  $\delta$  = 3.54 (s, 6 H,  $-\text{CH}_3$ ), 4.40 (s, 4 H,  $-\text{CH}_2-\text{CH}_2-$ ), 7.02 (d, 2 H,  $-\text{CH}=\text{CH}-$ , <sup>3</sup>*J*(H,H) = 2.1 Hz), 7.29 (d, 2 H,  $-\text{CH}=\text{CH}-$ , <sup>3</sup>*J*(H,H) = 2.1 Hz) ppm. <sup>31</sup>P{<sup>1</sup>H} NMR (DMSO, 161.9 MHz):  $\delta$  = -144.1 (q, 1 P) ppm. <sup>19</sup>F NMR (DMSO, 376.48 MHz):  $\delta$  = -70.1 (d, 6 F, <sup>1</sup>*J*(P,F) = 711.3 Hz) ppm.

$[\text{Tl}\{\text{Au}(\text{C}_6\text{Cl}_5)_2\}(\text{L1})]$  (**3**) and  $[\text{Tl}\{\text{Au}(\text{C}_6\text{Cl}_5)_2\}(\text{L2})]$  (**4**):  $[\text{Tl}\{\text{Au}(\text{C}_6\text{Cl}_5)_2\}]_n$  (0.167 mmol, 150.0 mg) was added to a suspension of **L1** (0.167 mmol, 55.7 mg) or **L2** (0.167 mmol, 58.0 mg) in tetrahydrofuran. After 1 h of stirring, the solution was concentrated under vacuum. Finally, the addition of dichloromethane (5 mL) led to the precipitation of products **3** or **4** as orange solids.

**Compound 3:** Yield 84%.  $\text{C}_{21}\text{H}_{12}\text{AuCl}_{10}\text{N}_4\text{Se}_2\text{Tl}$  (1234.14); calcd. C 20.44, H 0.98, N 4.54; found C 20.80, H 1.05, N 4.77.  $A_M$  (acetone) =  $99.0 \Omega^{-1} \text{cm}^2 \text{mol}^{-1}$ . <sup>1</sup>H NMR (300 MHz,  $[\text{D}_6]\text{acetone}$ ):  $\delta$  = 7.89 (2 H), 7.24 (2 H), 6.51 (s, 2 H,  $\text{CH}_2$ ), 3.65 (s, 6 H,  $\text{CH}_3$ ) ppm. MALDI-TOF(-): *m/z* (%) = 695  $[\text{Au}(\text{C}_6\text{Cl}_5)_2]^-$  (100). MALDI-TOF(+): *m/z* (%) = 534  $[\text{Tl}(\text{L1})]^+$  (100). FTIR (Nujol):  $\tilde{\nu}$  = 835 and  $613 \text{ cm}^{-1}$  ( $[\text{Au}(\text{C}_6\text{Cl}_5)_2]$ ).

**Compound 4:** Yield 70%.  $\text{C}_{22}\text{H}_{14}\text{AuCl}_{10}\text{N}_4\text{Se}_2\text{Tl}$  (1248.17); calcd. C 21.17, H 1.13, N 4.49; found C 20.90, H 1.14, N 4.20.  $A_M$  (acetone) =  $109.5 \Omega^{-1} \text{cm}^2 \text{mol}^{-1}$ . <sup>1</sup>H NMR (300 MHz,  $[\text{D}_6]\text{acetone}$ ):  $\delta$  = 7.26 (2 H), 7.08 (2 H), 4.63 (s, 4 H,  $\text{CH}_2$ ), 3.65 (s, 6 H,  $\text{CH}_3$ ) ppm.

MALDI-TOF(-):  $m/z$  (%) = 695  $[\text{Au}(\text{C}_6\text{Cl}_5)_2]^-$  (100). MALDI-TOF(+):  $m/z$  (%) = 553  $[\text{Ti}(\text{L}2)]^+$  (100). FTIR (Nujol):  $\tilde{\nu}$  = 836 and  $614\text{ cm}^{-1}$   $[\text{Au}(\text{C}_6\text{Cl}_5)_2]$ .

**Computational Details:** For DFT and time-dependent DFT calculations, the model system of the ligand **L1a** was optimized at the DFT level of theory using the TURBOMOLE program package. For this optimization we used the B3-LYP and BH-LYP functionals<sup>[43]</sup> as implemented in TURBOMOLE.<sup>[44]</sup> The electronic structures for complexes **1** and **3** were calculated by single-point DFT calculations on model systems **1a** and **3a** built up from the X-ray diffraction results. Calculations were performed without any assumption of symmetry.

The excitation energies were obtained at the density functional level by using the time-dependent approach,<sup>[45–49]</sup> which is a DFT generalization of the Hartree–Fock linear response (HFLR) or random-phase approximation (RPA) method.<sup>[50]</sup>

In all calculations, the Karlsruhe split-valence quality basis sets<sup>[51]</sup> augmented with polarization functions<sup>[52]</sup> were used (SVP). The Stuttgart effective core potentials in TURBOMOLE were used for Au and Ti.<sup>[53]</sup>

**Crystallography:** The crystals were mounted in inert oil on glass fibres and transferred to the cold gas stream of an Oxford Diffraction Xcalibur (for the crystals of complex **1**) or a Nonius Kappa CCD diffractometer (**3**) equipped with an Oxford Instruments low-temperature attachment. Data were collected by monochromated Mo- $K_\alpha$  radiation ( $\lambda = 0.71073\text{ \AA}$ ). Scan type  $\omega$  and  $\phi$ . Absorption corrections based on multiple scans were applied with the program SADABS (for the crystal structure of complex **1**) or SORTAV (**3**). The structures were solved by direct methods and refined on  $F^2$  using the program SHELXL-97.<sup>[54]</sup> All non-hydrogen atoms were anisotropically refined. Hydrogen atoms were included using a riding model.

CCDC-805083 (for **1**) and -805084 (for **3**) contain the supplementary crystallographic data for this paper. These data can be obtained free of charge from The Cambridge Crystallographic Data Centre via [www.ccdc.cam.ac.uk/data\\_request/cif](http://www.ccdc.cam.ac.uk/data_request/cif).

**Crystal Data for the Crystal Structure of Complex 1:**  $\text{C}_6\text{H}_{12}\text{F}_6\text{N}_4\text{Se}_2\text{Ti}\cdot\text{CH}_3\text{CN}$ ,  $M_r = 724.54$ ; orthorhombic,  $Pbca$ ,  $a = 8.5981(17)\text{ \AA}$ ,  $b = 18.510(4)\text{ \AA}$ ,  $c = 24.425(5)\text{ \AA}$ ,  $V = 3883.3(13)\text{ \AA}^3$ ,  $Z = 8$ ,  $\rho_{\text{calcd.}} = 2.479\text{ g cm}^{-3}$ ,  $\mu(\text{Mo-}K_\alpha) = 12.211\text{ mm}^{-1}$ ,  $R1 = 0.0255$ ,  $wR2 = 0.0567$  for 53764 observed reflections [ $I > 2\sigma(I)$ ].

**Crystal Data for 3:**  $\text{C}_{21}\text{H}_{12}\text{AuCl}_{10}\text{N}_4\text{Se}_2\text{Ti}$ ,  $M_r = 1234.10$ , triclinic,  $P\bar{1}$ ,  $a = 11.0840(11)\text{ \AA}$ ,  $b = 11.5294(9)\text{ \AA}$ ,  $c = 13.6587(14)\text{ \AA}$ ,  $\alpha = 109.604(6)^\circ$ ,  $\beta = 94.018(3)^\circ$ ,  $\gamma = 103.448(5)^\circ$ ,  $V = 1578.2(3)\text{ \AA}^3$ ,  $Z = 2$ ,  $\rho_{\text{calcd.}} = 2.597\text{ g cm}^{-3}$ ,  $\mu(\text{Mo-}K_\alpha) = 12.917\text{ mm}^{-1}$ ,  $R1 = 0.0691$ ,  $wR2 = 0.1852$  for 17919 observed reflections [ $I > 2\sigma(I)$ ].

**Supporting Information** (see footnote on the first page of this article): DFT and TD-DFT results for all model systems using BH-LYP functional and TZVP basis sets for the case of the free ligand.

## Acknowledgments

This work was supported by the Ministerio de Educación y Ciencia (MEC), Dirección General de Investigación (DGI)/Fondos Europeos para el Desarrollo Regional (FEDER) (CTQ2010-20500-C02-01 and CTQ2010-20500-C02-02). T. L. thanks Ministerio de Ciencia e Innovación (MICINN) for a grant. M. A. and V. L. thank the Università degli Studi di Cagliari for financial support.

- [1] a) P. Pyykkö, *Chem. Rev.* **1997**, *97*, 597; b) T. Schwabe, S. Grimme, J. P. Djukic, *J. Am. Chem. Soc.* **2009**, *131*, 14156.
- [2] a) H. Schmidbaur, *Gold Bull.* **2000**, *33*, 3; b) F. Scherbaum, A. Grömann, B. Huber, C. Krüger, H. Schmidbaur, *Angew. Chem. Int. Ed. Engl.* **1988**, *27*, 1544; c) F. Scherbaum, A. Grömann, G. Müller, H. Schmidbaur, *Angew. Chem. Int. Ed. Engl.* **1989**, *28*, 463; d) H. Schmidbaur, F. Scherbaum, B. Hubert, G. Müller, *Angew. Chem. Int. Ed. Engl.* **1988**, *27*, 419.
- [3] See, for example: a) H. H. Karsch, U. Schubert, *Z. Naturforsch., Teil B* **1982**, *37*, 186; b) T. Tsuda, S. Ohba, M. Takahashi, M. Ito, *Acta Crystallogr., Sect. C* **1989**, *45*, 887; c) M. Jansen, *Angew. Chem. Int. Ed. Engl.* **1987**, *26*, 1098.
- [4] See, for example: A. Heine, R. Herbst-Irmer, D. Stalke, *J. Chem. Soc., Chem. Commun.* **1993**, 1729.
- [5] See, for example: H. Schmidbaur, H.-J. Öller, D. L. Wilkinson, B. Huber, G. Müller, *Chem. Ber.* **1989**, *122*, 31.
- [6] See, for example: S. Otsuka, *J. Organomet. Chem.* **1980**, *200*, 191.
- [7] Y.-L. Pan, J. T. Mage, M. J. Fink, *J. Am. Chem. Soc.* **1993**, *115*, 3842.
- [8] See, for example: a) T. Tanase, Y. Kudo, M. Ohno, K. Kobayashi, Y. Yamamoto, *Nature* **1990**, *344*, 526; b) N. M. Boag, M. Green, J. A. K. Howard, F. G. A. Stone, H. Wade, *J. Chem. Soc., Dalton Trans.* **1981**, 862.
- [9] See, for example: a) R. Blom, H. Werner, J. Wolf, *J. Organomet. Chem.* **1988**, *354*, 293; b) H. Pritzkow, P. Jennische, *Acta Chem. Scan. Ser. A* **1975**, *29*, 60; c) B. Krebs, H. Greiwing, *Z. Anorg. Allg. Chem.* **1992**, *616*, 145.
- [10] See, for example: L. A. Bengtsson, R. Hoffmann, *J. Am. Chem. Soc.* **1993**, *115*, 2666.
- [11] See, for example: J. K. Nagle, A. L. Balch, M. M. Olmstead, *J. Am. Chem. Soc.* **1988**, *110*, 319.
- [12] A. L. Balch, B. J. Davis, E. Y. Fung, M. M. Olmstead, *Inorg. Chim. Acta* **1993**, *212*, 149.
- [13] A. L. Balch, J. K. Nagle, M. M. Olmstead, P. E. Reedy Jr., *J. Am. Chem. Soc.* **1987**, *109*, 4123.
- [14] See, for example: S. Wang, J. P. Fackler Jr., C. King, J. C. Wang, *J. Am. Chem. Soc.* **1988**, *110*, 3308.
- [15] S. Wang, G. Garzón, C. King, J. C. Wang, J. P. Fackler Jr., *Inorg. Chem.* **1989**, *28*, 4623.
- [16] See, for example: J. C. Jeffery, P. A. Jelliss, F. G. A. Stone, *Inorg. Chem.* **1993**, *32*, 3943.
- [17] T. F. Carlson, J. P. Fackler Jr., R. J. Staples, R. E. P. Winpenny, *Inorg. Chem.* **1995**, *34*, 426.
- [18] H.-K. Yip, H.-M. Lin, Y. Wang, C.-M. Che, *J. Chem. Soc., Dalton Trans.* **1993**, 2939.
- [19] O. Crespo, A. Laguna, E. J. Fernández, J. M. López-de-Luzuriaga, P. G. Jones, M. Teichert, M. Monge, P. Pyykkö, N. Runeberg, M. Schütz, H.-J. Werner, *Inorg. Chem.* **2000**, *39*, 4786.
- [20] a) P. Pyykkö, *Angew. Chem. Int. Ed.* **2004**, *43*, 4412; b) P. Pyykkö, *Inorg. Chim. Acta* **2005**, *358*, 4113; c) P. Pyykkö, *Chem. Soc. Rev.* **2008**, *37*, 1967.
- [21] a) P. Schwerdtfeger, *Inorg. Chem.* **1991**, *30*, 64; b) G. Treboux, J. C. Barthelat, *J. Am. Chem. Soc.* **1993**, *115*, 4870; c) C. Janiak, R. Hoffmann, *J. Am. Chem. Soc.* **1990**, *112*, 5024.
- [22] P. Pyykkö, M. Straka, T. Tamm, *Phys. Chem. Chem. Phys.* **1999**, *1*, 3441.
- [23] <http://www.webelements.com>.
- [24] E. J. Fernández, A. Laguna, J. M. López-de-Luzuriaga, F. Mendizábal, M. Monge, E. Olmos, J. Pérez, *Chem. Eur. J.* **2003**, *9*, 456.
- [25] a) E. J. Fernández, J. M. López-de-Luzuriaga, M. Monge, M. E. Olmos, J. Pérez, A. Laguna, A. A. Mohamed, J. P. Fackler Jr., *J. Am. Chem. Soc.* **2003**, *125*, 2022; b) E. J. Fernández, J. M. López-de-Luzuriaga, M. Monge, M. Montiel, M. E. Olmos, J. Pérez, A. Laguna, F. Mendizábal, A. A. Mohamed, J. P. Fackler Jr., *Inorg. Chem.* **2004**, *43*, 3573; c) J. M. López-de-Luzuriaga in *Modern Supramolecular Gold Chemis-*

- try (Ed.: A. Laguna), Wiley-VCH, Weinheim, Germany, **2008**, p. 347.
- [26] F. Weisbrock, H. Schmidbaur, *J. Am. Chem. Soc.* **2003**, *125*, 3622, and references therein.
- [27] E. J. Fernández, A. Laguna, J. M. López-de-Luzuriaga, *Dalton Trans.* **2007**, 1969.
- [28] a) W. G. Jia, Y. B. Huang, Y. J. Lin, G. L. Wang, G.-X. Jin, *Eur. J. Inorg. Chem.* **2008**, 4063; b) W. G. Jia, Y. B. Huang, Y. J. Lin, G.-X. Jin, *Dalton Trans.* **2008**, 5612.
- [29] G. Zahn, A. Franke, W. Dietzsch, *Acta Crystallogr., Sect. C* **1995**, *51*, 854.
- [30] H.-U. Hummel, E. Fischer, T. Fischer, D. Größ, A. Franke, W. Dietzsch, *Chem. Ber.* **1992**, *125*, 1565.
- [31] E. J. Fernández, A. Garau, A. Laguna, T. Lasanta, V. Lippolis, J. M. López-de-Luzuriaga, M. Montiel, M. E. Olmos, *Organometallics* **2010**, *29*, 2951.
- [32] E. J. Fernández, A. Laguna, J. M. López-de-Luzuriaga, M. Monge, M. Montiel, M. E. Olmos, J. Pérez, *Organometallics* **2004**, *23*, 774.
- [33] O. Crespo, E. J. Fernández, P. G. Jones, A. Laguna, J. M. López-de-Luzuriaga, A. Mendía, M. Monge, M. E. Olmos, *Chem. Commun.* **1998**, 2233.
- [34] E. J. Fernández, A. Laguna, J. M. López-de-Luzuriaga, M. Montiel, M. E. Olmos, J. Pérez, *Inorg. Chim. Acta* **2005**, *358*, 4293.
- [35] E. J. Fernández, A. Laguna, J. M. López-de-Luzuriaga, M. Montiel, M. E. Olmos, J. Pérez, *Organometallics* **2005**, *24*, 1631.
- [36] E. J. Fernández, A. Laguna, J. M. López-de-Luzuriaga, M. E. Olmos, J. Pérez, *Dalton Trans.* **2004**, 1801.
- [37] E. J. Fernández, P. G. Jones, A. Laguna, J. M. López-de-Luzuriaga, M. Monge, M. Montiel, M. E. Olmos, J. Pérez, *Z. Naturforsch., Teil B* **2004**, *59*, 1379.
- [38] E. J. Fernández, P. G. Jones, A. Laguna, J. M. López-de-Luzuriaga, M. Monge, M. E. Olmos, J. Pérez, *Inorg. Chem.* **2002**, *41*, 1056.
- [39] E. J. Fernández, A. Laguna, T. Lasanta, J. M. López-de-Luzuriaga, M. Montiel, M. E. Olmos, *Organometallics* **2008**, *27*, 2971.
- [40] A search in the CSD (version 5.32, year 2011) made on all the compounds containing a CH<sub>2</sub>...Se intermolecular contact shorter or equal to the sum of van der Waals radii (810 structures,  $R < 0.05$ ) showed that the H...Se distances range between 2.70 and 3.10 Å with a mean value of 3.00 Å, and the C-H...Se angles range between 105.8 and 178.5° with a mean value of 147.0°. See also: M. Iwaoka, S. Tomoda, *J. Am. Chem. Soc.* **1994**, *116*, 4463.
- [41] a) E. J. Fernández, A. Laguna, J. M. López-de-Luzuriaga, M. Monge, M. E. Olmos, J. Pérez, *J. Am. Chem. Soc.* **2002**, *124*, 5942; b) E. J. Fernández, J. M. López-de-Luzuriaga, M. E. Olmos, J. Pérez, A. Laguna, M. C. Lagunas, *Inorg. Chem.* **2005**, *44*, 6012.
- [42] a) M. C. Aragoni, M. Arca, A. J. Blake, F. A. Devillanova, W. W. du Mont, A. Garau, F. Isaia, V. Lippolis, G. Verani, C. Wilson, *Angew. Chem. Int. Ed.* **2001**, *40*, 4229; b) V. V. Namboodiria, R. S. Varma, *Org. Lett.* **2002**, *4*, 3161.
- [43] a) A. D. Becke, *J. Chem. Phys.* **1992**, *96*, 215; b) A. D. Becke, *J. Chem. Phys.* **1993**, *98*, 5648; c) C. Lee, W. Yang, R. G. Parr, *Phys. Rev. Lett.* **1998**, *B37*, 785; d) A. D. Becke, *J. Chem. Phys.* **1993**, *98*, 1372.
- [44] R. Ahlrichs, M. Bär, M. Häser, H. Horn, C. Kölmel, *Chem. Phys. Lett.* **1989**, *162*, 165.
- [45] R. Bauernschmitt, R. Ahlrichs, *Chem. Phys. Lett.* **1996**, *256*, 454.
- [46] R. Bauernschmitt, R. Ahlrichs, *J. Chem. Phys.* **1996**, *104*, 9047.
- [47] R. Bauernschmitt, M. Häser, O. Treutler, R. Ahlrichs, *Chem. Phys. Lett.* **1997**, *264*, 573 and refs. therein.
- [48] E. K. U. Gross, W. Kohn, *Advan. Quantum Chem.* **1990**, *21*, 255.
- [49] M. E. Casida, in: *Recent Advances in Density Functional Methods*, vol. 1 (Ed.: D. P. Chong), World Scientific, **1995**.
- [50] J. Olsen, P. Jørgensen, in: *Modern Electronic Structure Theory*, vol. 2 (Ed.: D. R. Yarkony), World Scientific, **1995**.
- [51] A. Schäfer, H. Horn, R. Ahlrichs, *J. Chem. Phys.* **1992**, *97*, 2571.
- [52] T. H. Dunning Jr., *J. Chem. Phys.* **1994**, *100*, 5829.
- [53] D. Andrae, U. Haeussermann, M. Dolg, H. Stoll, H. Preuss, *Theor. Chim. Acta* **1990**, *77*, 123.
- [54] G. M. Sheldrick, *SHELXL-97*, Program for Crystal Structure Refinement, University of Göttingen, Germany, **1997**.

Received: January 4, 2011

Published Online: April 4, 2011